Lower and upper bounds for the absolute free energy by the hypothetical scanning Monte Carlo method: Application to liquid argon and water

Ronald P. White and Hagai Meirovitch[a)]
Center for Computational Biology and Bioinformatics and Department of Molecular Genetics & Biochemistry, University of Pittsburgh School of Medicine, W1058 BST, Pittsburgh, Pennsylvania 15261

(Received 27 July 2004; accepted 16 September 2004)

The hypothetical scanning (HS) method is a general approach for calculating the *absolute* entropy S and free energy F by analyzing Boltzmann samples obtained by Monte Carlo or molecular dynamics techniques. With HS applied to a fluid, each configuration i of the sample is reconstructed by gradually placing the molecules in their positions at i using transition probabilities (TPs). At each step of the process the system is divided into two parts, the already treated molecules (the ''past''), which are fixed, and the as yet unspecified (mobile) ''future'' molecules. Obtaining the TP exactly requires calculating partition functions over all positions of the future molecules in the presence of the frozen past, thus it is customary to invoke various approximations to best represent these quantities. In a recent publication [Proc. Natl. Acad. Sci. USA **101**, 9235 (2004)] we developed a version of HS called *complete* HSMC, where each TP is calculated from an MC simulation involving all of the future molecules (the *complete* future); the method was applied very successfully to Lennard-Jones systems (liquid argon) and a box of TIP3P water molecules. In its basic implementation the method provides lower and upper bounds for F, where the latter can be evaluated only for relatively small systems. Here we introduce a new expression for an upper bound, which can be evaluated for larger systems. We also propose a new exact expression for F and verify its effectiveness. These free energy functionals lead to significantly improved accuracy (as applied to the liquid systems above) which is comparable to our thermodynamic integration results. We formalize and discuss theoretical aspects of HSMC that have not been addressed in previous studies. Additionally, several functionals are developed and shown to provide the free energy through the analysis of a single configuration. © *2004 American Institute of Physics.*
[DOI: 10.1063/1.1814355]

I. INTRODUCTION

The *absolute* entropy S and the Helmholtz free energy F are fundamental quantities in statistical mechanics as S is a measure of order and F is the correct criterion of stability. The free energy is required, for example, in determining the relative populations of protein structures. However, calculation of these quantities for a complex system such as a peptide or a protein in water by computer simulation is an extremely difficult problem.[1–4] S and F are related through the definition $F=E-TS$, where T is the absolute temperature and E is the average energy. Calculation of E using any simulation technique is fairly straightforward, where E_i is ''written'' on system configuration i in terms of microscopic interactions (e.g., Lennard-Jones interactions of argon). On the other hand, calculating $S(\sim -\ln P_i^B)$ or F requires knowledge of the *value* of the Boltzmann probability P_i^B. This sampling probability is not provided directly by the commonly used *dynamical* techniques, Metropolis Monte Carlo (MC),[5] and molecular dynamics.[6,7] In most cases calculation of F is based on reversible thermodynamic integration (TI) techniques which provide the difference in the free energy, $\Delta F_{m,n}$, between two states m and n (e.g., the helical and hairpin states of a peptide) and only when the absolute entropy of one state is known, that of the other can be obtained. While TI is a robust approach (see Refs. 1–4, 8, 9 and references cited therein), for proteins, such integration is feasible only if the structural variance between the two states is very small; otherwise, the integration path can become prohibitively lengthy and complex. Therefore, it is important to develop methods that provide P_i^B at least approximately, enabling one to calculate the absolute F_m and F_n from two samples of the states m and n; in this case $\Delta F_{m,n}=F_m-F_n$ can be calculated even for *significantly different* states since the integration process is avoided.

Meirovitch has proposed a unique approach for calculating the absolute entropy, where two related approximate techniques, the local states method[10–14] and the hypothetical scanning (HS) method[15–17] have been developed and applied to magnetic systems, polymers, and peptides. Our long-term goal is to be able to calculate the absolute free energy of a peptide or a surface loop of a protein immersed in explicit water. Therefore, in recent studies, as a first step, the HS method has been extended to liquid argon in two different approximations, one called grand canonical HS (Ref. 8) and the other Monte Carlo HS (HSMC).[9] While very good results

a)Author to whom correspondence should be addressed. Electronic mail: hagaim@pitt.edu

were obtained, in some cases better accuracy would be needed. An additional issue is that the methods are implemented with boundary conditions that are different from those used to generate the analyzed sample (typically periodic boundary conditions). This inconsistency, along with the way the TPs are calculated in general, makes these methods inconvenient to apply to inhomogeneous system, such as a peptide in water. Therefore, recently we have developed HSMC further to a method called *complete* HSMC that does not have the above inconsistency, and its accuracy increases indefinitely with increasing MC sampling. The method was applied[18] to argon systems of different size, and to a system of 64 TIP3P water molecules,[19] and in a related paper it was also extended to peptides.[20]

In this paper complete HSMC is further developed and its accuracy is enhanced significantly as applied to the same argon systems and TIP3P water studied in Ref. 18. Whereas in its basic implementation the method leads to a lower bound of the free energy (an upper bound for S), in this paper we develop an efficient way to calculate an upper bound for F as well. We also study the efficiency of a new expression for the *correct* F and demonstrate that the free energy can be obtained from a *single* structure, an important feature that ultimately would make our approach convenient to treat peptides in explicit water. In the following section we describe the complete HSMC method as applied to liquids, followed by the presentation of the results in Sec. III. As only the ''complete'' variant of HSMC is studied in the present work, for brevity, it will simply be referred to as HSMC.

II. THEORY AND IMPLEMENTATION

A. Free energy and its fluctuation

We start by defining the free energy and discussing some of its properties. For simplicity we consider a discrete system of configurations, i, with energy E_i. The Boltzmann probability P_i^B is

$$P_i^B=\frac{\exp[-E_i/k_BT]}{Z}, \tag{1}$$

where k_B is the Boltzmann constant, T is the absolute temperature, and Z is the partition function. Using P_i^B, the ensemble average energy $\langle E\rangle$ is given by

$$\langle E\rangle=\sum_i P_i^B E_i. \tag{2}$$

The entropy S and free energy F can also be formally expressed as ensemble averages,

$$S=\langle S\rangle=-k_B\sum_i P_i^B \ln P_i^B \tag{3}$$

and

$$F=\langle F\rangle=\sum_i P_i^B[E_i+k_BT\ln P_i^B]=\langle E\rangle-TS. \tag{4}$$

An extremely important property of this representation of F (but not other representations) is that its variance vanishes, $\sigma^2(F)=0$; indeed, substituting the expression for P_i^B in the brackets [Eq. (4)] leads to a constant, $-k_BT\ln Z$ for any i.[17,21] This means that the *exact* free energy can be obtained from a *single* structure i if P_i^B is known. Moreover, while F is an extensive variable, its zero fluctuation property holds for any number of atoms N. This important property is not shared by the entropy and the energy—their fluctuations increase as $\sim N^{1/2}$, and therefore it is difficult to estimate them accurately for a large system.

In practice, however, evaluation of P_i^B in simulations will always be approximate. In particular, with the HS method, approximate probabilities P_i^{HS} are determined, and thereby give rise to approximate entropy and free energy functionals, S^A and F^A,

$$S^A=-k_B\sum_i P_i^B \ln P_i^{\mathrm{HS}} \tag{5}$$

and

$$F^A=\sum_i P_i^B[E_i+k_BT\ln P_i^{\mathrm{HS}}]=\langle E\rangle-TS^A, \tag{6}$$

where i runs over the entire ensemble. Using Jensen's inequality, S^A can be shown rigorously to be an upper bound[16] for the correct entropy S (see also the Appendix), thus F^A is a lower bound of F. P_i^{HS} is generally a function of a set of parameters or running conditions, denoted by α (e.g., see Refs. 8 and 9), which effectively determine its accuracy, the better the approximation the smaller is S^A, and the larger is F^A. The dependence of these functionals (and others introduced below) on the chosen approximation α is fundamental, and at times we will write $S^A(\alpha)$ and $F^A(\alpha)$ explicitly.

It is important to note that the quantity $F_i^{\mathrm{HS}}=[E_i+k_BT\ln P_i^{\mathrm{HS}}]$ in Eq. (6) is not the same for all i, meaning that the fluctuation, σ_A in F^A is not zero. This fluctuation, which is defined by

$$\sigma_A=\left[\sum_i P_i^B[F^A-F_i^{\mathrm{HS}}]^2\right]^{1/2}$$
$$=\left[\sum_i P_i^B[F^A-E_i-k_BT\ln P_i^{\mathrm{HS}}]^2\right]^{1/2}, \tag{7}$$

is however expected to decrease as the approximation improves, meaning that for very good approximations of P_i^{HS}, the free energy can be very accurately determined by averaging F_i^{HS} over just a handful of configurations (or even a single one). The HSMC method can provide this accuracy, and very good values for the free energy have been obtained from a small number of configurations.

B. Upper bounds for the free energy

One can define another approximate free energy functional denoted F^B,[16]

$$F^B=\sum_i P_i^{\mathrm{HS}}[E_i+k_BT\ln P_i^{\mathrm{HS}}]. \tag{8}$$

According to the free energy minimum principle,[22] $F^B\geqslant F$ [Eq. (4)]. Thus, F^B is an upper bound which approaches the correct free energy F when $P_i^{\mathrm{HS}}\rightarrow P_i^B$ [Eq. (1)]. It is necessary to rewrite Eq. (8) such that F^B can be estimated by

importance sampling from a (Boltzmann) sample of configurations generated with P_i^B (rather than P_i^{HS}). Applying the identities $\Sigma_i P_i^{\mathrm{HS}}=1$ and $P_i^B/(\exp[-E_i/k_BT]/Z)=P_i^B/P_i^B=1$, one obtains

$$F^B=\frac{\Sigma_i P_i^B[P_i^{\mathrm{HS}}\exp(E_i/k_BT)(E_i+k_BT\ln P_i^{\mathrm{HS}})]}{\Sigma_i P_i^B[P_i^{\mathrm{HS}}\exp(E_i/k_BT)]}. \tag{9}$$

In practice, F^B is estimated as the ratio of simple arithmetic averages, which are accumulated for each of the quantities in the brackets in Eq. (9). It should be noted, however, that the statistical reliability of this estimation (unlike the estimation of F^A) decreases sharply with increasing system size, because the overlap between the probability distributions P_i^B and P_i^{HS} decreases exponentially (see discussion in Ref. 13).

Another way to estimate F^B is by using a "reversed-Schmidt procedure,"[13,16] which enables one to extract from the given *unbiased* sample of size n generated with P_i^B an effectively smaller *biased* sample generated with P_i^{HS}. Thus, the configurations of the unbiased sample are treated consecutively. If a configuration i was accepted to the biased sample, the next configuration j would be accepted with a transition probability A_{ij},

$$A_{ij}=\min\{1,\exp[(E_j-E_i)/k_BT]P_j^{\mathrm{HS}}/P_i^{\mathrm{HS}}\}. \tag{10}$$

Equation (10) is a generalized MC procedure, which satisfies the detailed balance condition and is carried out with random numbers. The acceptance rate R provides a measure for the *effective size* of the accepted biased sample,

$$R=n_{\mathrm{accept}}/n, \tag{11}$$

where n_{accept} is the number of accepted configurations. The effectiveness of this procedure is again limited by the overlap of the distributions, P_i^B and P_i^{HS}, and we will in fact only report F^B results as calculated with Eq. (9). We will still, however, apply the reversed-Schmidt procedure to the same sample of results, and report the acceptance rate, R, which is a useful gauge of the reliability of the F^B value (calculated with either method). Thus, the closer is R to 1 the better is the overlap between P_i^B and P_i^{HS}, the closer is F^B to F, and the smaller is the sample size required to estimate F^B reliably.

With values for both F^A and F^B, their average, F^M, defined by

$$F^M=(F^A+F^B)/2, \tag{12}$$

often becomes a better approximation than either of them individually. This is provided that their deviations from F (in magnitude) are approximately equal, and that the statistical error in F^B is not too large. Typically, several improving approximations for F^A, F^B, and F^M are calculated as a function of α, and their convergence enables one to determine the correct free energy with high accuracy.

C. A Gaussian estimation of F^B

We now describe an efficient method to estimate the free energy upper bound, F^B [Eqs. (8) and (9)], which can effectively overcome the statistical limitations associated with the standard evaluations of F^B described in the preceding section. It is noted that the applicability of this method is dependent on the (form of the) HS implementation. The HSMC method of the present work is particularly well suited to the required assumptions, and reasons for this are discussed in Sec. II M and in the Appendix.

We begin by rewriting Eq. (9) as

$$F^B=\frac{\Sigma_i P_i^B\exp[F_i^{\mathrm{HS}}/k_BT][F_i^{\mathrm{HS}}]}{\Sigma_i P_i^B\exp[F_i^{\mathrm{HS}}/k_BT]}, \tag{13}$$

where we have used $F_i^{\mathrm{HS}}=[E_i+k_BT\ln P_i^{\mathrm{HS}}]$. Equation (13) emphasizes an *explicit* dependence of F^B on the variable, F_i^{HS}, a quantity that is directly related to the average, F^A [Eq. (6)], and the fluctuation, σ_A [Eq. (7)]. Let us now assume that when configurations i are sampled from the Boltzmann distribution (i.e., with P_i^B), their corresponding F_i^{HS} values occur with a Gaussian probability. That is, the resulting F_i^{HS} values are described by the Gaussian distribution,

$$\rho(F_i^{\mathrm{HS}})=\rho(F')=\frac{1}{\sqrt{2\pi}\sigma_A}\exp[-(F'-F^A)^2/2(\sigma_A)^2], \tag{14}$$

which is thus determined solely by the two parameters, F^A (the mean) and σ_A (the standard deviation). Now, rather than summing over the configurations i with their weights, P_i^B, as in Eq. (13), we can sum (integrate) over all values of F_i^{HS} weighted with $\rho(F_i^{\mathrm{HS}})$. The numerator in Eq. (13) becomes

$$\begin{aligned}\sum_i P_i^B\exp[F_i^{\mathrm{HS}}/k_BT][F_i^{\mathrm{HS}}]&\approx\frac{1}{\sqrt{2\pi}\sigma_A}\int(\exp[F'/k_BT][F'])\\&\quad\times\exp[-(F'-F^A)^2/2(\sigma_A)^2]dF'\\&=\left(\frac{(\sigma_A)^2}{k_BT}+F^A\right)\exp\left[\frac{1}{2}\left(\frac{\sigma_A}{k_BT}\right)^2+\frac{F^A}{k_BT}\right],\end{aligned} \tag{15}$$

and the denominator is

$$\begin{aligned}\sum_i P_i^B\exp[F_i^{\mathrm{HS}}/k_BT]&\approx\frac{1}{\sqrt{2\pi}\sigma_A}\int(\exp[F'/k_BT])\\&\quad\times\exp[-(F'-F^A)^2/2(\sigma_A)^2]dF'\\&=\exp\left[\frac{1}{2}\left(\frac{\sigma_A}{k_BT}\right)^2+\frac{F^A}{k_BT}\right].\end{aligned} \tag{16}$$

The ratio of the results in Eqs. (15) and (16), is the new (Gaussian) estimation of F^B, denoted F_{G}^B,

$$F_{\mathrm{G}}^B=\frac{(\sigma_A)^2}{k_BT}+F^A. \tag{17}$$

We see that F_{G}^B depends only on F^A and on the fluctuation σ^A. This is an advantage of F_{G}^B because these quantities are typically easier to estimate than F^B from Eq. (9) or (10). Provided that the Boltzmann sample of F_i^{HS} values (for some

parameter set α) is approximately Gaussian, then $F_{\mathrm{G}}^{B} \approx F^{B}$. Our results show that this Gaussian distribution is a very good approximation as there is excellent agreement of F_{G}^{B} with F^{B} for cases where F^{B} is well converged.

Similar to Eq. (12) we define the average,

$$F_{\mathrm{G}}^{M} = (F^{A} + F_{\mathrm{G}}^{B})/2 = F^{A} + \frac{1}{2}\frac{(\sigma_A)^2}{k_B T}, \tag{18}$$

where again, several approximations for F^{A}, F_{G}^{B}, and F_{G}^{M} can be calculated as a function of α, and their convergence leads to highly accurate free energy determination.

D. Exact expression for the free energy

The denominator of F^{B} in Eqs. (9) and (13) defines an exact expression for the partition function,

$$\frac{1}{Z} = \frac{1}{Z}\sum_i P_i^B (P_i^{\mathrm{HS}}/P_i^B)$$

$$= \sum_i P_i^B (P_i^{\mathrm{HS}} \exp[E_i/k_B T])$$

$$= \sum_i P_i^B \exp[F_i^{\mathrm{HS}}/k_B T], \tag{19}$$

which is based on $\Sigma_i P_i^B (P_i^{\mathrm{HS}}/P_i^B) = 1$; therefore, Eq. (19) will hold for any approximation α as long as the $P_i^{\mathrm{HS}}(\alpha)$ are normalized, and an *exact* expression for the correct free energy F, denoted by F^{D}, is

$$F^{D} = k_B T \ln\left(\frac{1}{Z}\right) = k_B T \ln\left[\sum_i P_i^B \exp(F_i^{\mathrm{HS}}/k_B T)\right]. \tag{20}$$

Note that while the (Boltzmann) average of the approximate F_i^{HS} values gives a bound for the free energy ($\Sigma_i P_i^B F_i^{\mathrm{HS}} = F^{A}$), the average of $\exp[F_i^{\mathrm{HS}}/k_B T]$ leads to the free energy exactly. In fact, using Eq. (20), it is easy to verify that F^{A} defines a lower bound (i.e., $F^{A} \leqslant F$), where we must have

$$\exp[F^{A}/k_B T] = \exp\left[\sum_i P_i^B (F_i^{\mathrm{HS}}/k_B T)\right]$$

$$\leqslant \sum_i P_i^B \exp[F_i^{\mathrm{HS}}/k_B T] = \exp[F/k_B T], \tag{21}$$

in accordance with Jensen's inequality, which states that $f(\langle x\rangle) \leqslant \langle f(x)\rangle$ for a convex function $f(x)$. (See also the Appendix.)

In practice, the efficiency of estimating F by F^{D} depends on the fluctuation of this statistical average, which is determined by the fluctuation of F_i^{HS} exponentiated. That is, if the fluctuations in F_i^{HS} are small, then the values for $\exp[F_i^{\mathrm{HS}}/k_B T]$ do not vary drastically, and the averages for F^{D} (and F^{B}) can be estimated reliably. Still (as for F^{B}), the direct calculation of F through F^{D} will not be as statistically reliable as the corresponding calculation for the lower bound estimate, F^{A}. Obviously, as $F_i^{\mathrm{HS}} \to F$ (i.e., $P_i^{\mathrm{HS}} \to P_i^B$) all fluctuations become zero and F can be obtained from a single configuration. It should be pointed out that Eq. (19) with $P_i^{\mathrm{HS}} = 1/V^N$ was suggested for a lattice gas long ago by Salsburg *et al.*[23] (N is the number of particles and V is the volume.) This choice, however, leads to an extremely inefficient estimation at room temperature and works only at very high T where the Boltzmann probability is represented more faithfully by $1/V^N$.

We note additionally that in Eq. (16) $1/Z$ was calculated with the Gaussian distribution, which is expected to improve the convergence over that of Eq. (19); the free energy calculated from this Gaussian expression for $1/Z$ is equal to F_{G}^{M} [Eq. (18)].

E. The correlation between σ_A and F^{A}

The zero fluctuation property of the correct free energy can be exploited directly through the extrapolation of a series of F^{A} values, which are derived from a set of improving approximations. Here the fluctuations are expected to decrease systematically as the approximation improves, and we write F^{A} as $F^{A}(\alpha)$ [and σ_A as $\sigma_A(\alpha)$], thus emphasizing the effect of the general parameter set α, which controls the level of approximation and therefore the quality of the free energy estimate. It has been suggested[17] to express the correlation between $F^{A}(\alpha)$ and $\sigma_A(\alpha)$ by the approximate function

$$F^{A}(\alpha) = F^{\mathrm{extp}} + C[\sigma_A(\alpha)]^{\gamma}, \tag{22}$$

where F^{extp} is the extrapolated value of the free energy, and C and γ are parameters to be optimized by best-fitting results for $F^{A}(\alpha)$ and $\sigma_A(\alpha)$ for different approximations α. One can also calculate the tangent to the function at $\sigma_A(\alpha_{\mathrm{best}})$, which is the lowest value for the fluctuation obtained from the best approximation, α_{best}. If Eq. (22) defines a concave-down function and this trend of $F^{A}(\sigma_A)$ is assumed to hold for better (uncalculated) approximations of F^{A}, the intersection of the tangent with the vertical axis [$\sigma_A = 0$] defines an upper bound for F, which is denoted F^{up}. This upper bound, along with the best value for the lower bound, $F^{A}(\alpha_{\mathrm{best}})$, can be used to define the average F^{M2},

$$F^{M2} = [F^{A}(\alpha_{\mathrm{best}}) + F^{\mathrm{up}}]/2. \tag{23}$$

F. Statistical mechanics of the liquid models

In this paper we study liquid models for argon and water. Argon is represented by the standard Lennard-Jones potential with the parameters $\epsilon/k_B = 119.8$ K and $\sigma = 3.405$ Å; water is represented by the three-site TIP3P potential.[19] We consider N atoms (molecules) enclosed in a box of volume, V, at temperature, T [(NVT) ensemble]. The configurational partition function is given by

$$Z_N = \int \exp[-E(\mathbf{x}^N)/k_B T] d\mathbf{x}^N, \tag{24}$$

where $E(\mathbf{x}^N)$ is the potential energy, $\mathbf{x}^N$ is the set of Cartesian and orientational (for water) coordinates, and $d\mathbf{x}^N$ is the corresponding differential (including any necessary Jacobian factors). The integration is carried out over the configurational space, V^N for argon, and $(8\pi^2 V)^N$ for water. Using the Boltzmann configurational probability density $\rho(\mathbf{x}^N)$,

$$\rho(\mathbf{x}^N) = \exp[-E(\mathbf{x}^N)/k_B T]/Z_N, \tag{25}$$

the total entropy S is

$$S=S_{\mathrm{IG}}+S_{\mathrm{e}}=S_{\mathrm{IG}}-k_B\int \rho(\mathbf{x}^N)\ln[(8\pi^2)^N V^N \rho(\mathbf{x}^N)]d\mathbf{x}^N, \tag{26}$$

where S_{IG} is the entropy of the ideal gas at the same temperature and density, and S_{e} is the excess entropy. The factor $(8\pi^2)^N$ would be replaced by unity for argon. The corresponding excess Helmholtz free energy is

$$F_{\mathrm{e}}=\int \rho(\mathbf{x}^N)(E(\mathbf{x}^N)+k_BT\ln[(8\pi^2)^N V^N \rho(\mathbf{x}^N)])d\mathbf{x}^N$$
$$=\langle E\rangle - TS_{\mathrm{e}}, \tag{27}$$

where $\langle E\rangle$ is the average potential energy. For water we present results for F_{e}; however, to be consistent with the literature, for argon the *configurational free energy* A_{c} (Ref. 24) is provided,

$$A_{\mathrm{c}}=-k_BT\ln\left(\frac{Z_N}{N!\,\sigma^{3N}}\right), \tag{28}$$

where σ is the van der Waals parameter from the Lennard-Jones potential.

G. The ideal HS method

It is helpful to explain the HSMC method developed in this paper by first describing an *ideal* (or ''perfect'') HS method, as applied to an *NVT* argon system with periodic boundary conditions simulated by MC; the extension for water is straightforward. It should first be pointed out that each argon configuration, in principle, could have been generated by an alternative *exact* build-up procedure, where argon atoms are added step-by-step to the initially empty volume (box) using transition probabilities (TPs). With the HS method the given MC sample is assumed to have been generated by this exact build-up procedure, and thus each configuration is reconstructed with this procedure, the TPs are calculated, and their product leads to $\rho(\mathbf{x}^N)$ and to the absolute entropy $\sim\ln\rho(\mathbf{x}^N)$.

In practice, the box is divided into $L^3=L\times L\times L$ cubic cells with a maximal size that still guarantees that no more than one center of a spherical argon molecule occupies a cell. (See Refs. 25–27 for other examples of cell approaches for fluid free energies.) During the analysis of configuration i, the cells are visited orderly line-by-line, layer-by-layer starting from one corner of the box until all of them have been treated. The calculation of TP_k for the target cell k [which could be a vacant $(-)$ or a populated cell $(+)$] is outlined as follows. At step k of the process, N_k atoms (i.e., occupied cells) and $k-1-N_k$ vacant cells have already been treated, i.e., their TPs have been calculated. These N_k atoms are now positioned at their coordinates of configuration i and together with the already visited vacant cells they define the (frozen) ''past.'' The $L^3-(k-1)$ as yet unvisited cells (including target cell k) define the ''future volume.'' To determine the TP of target cell k two *future* canonical partition functions are calculated, $Z^-(k)$ and $Z^+(k)$ for vacant and occupied cell k, respectively, by scanning all of the possible configurations of the remaining $N-N_k$ (future) atoms in the future volume, while the past volume is excluded, and for $Z^-(k)$, the target cell k is excluded as well. It is stressed that while the previously treated N_k atoms are fixed, their interactions with the future atoms are included in the calculation of $Z^-(k)$ and $Z^+(k)$.

The sum $Z^+(k)+Z^-(k)$ covers all possible future atomic arrangements at step k, therefore if cell k is vacant the TP_k is, $p(k,-)=Z^-(k)/[Z^+(k)+Z^-(k)]$. If on the other hand, cell k is occupied, then the future partition function, $Z^+(k,\mathbf{x}')$ is calculated where one of the future atoms is fixed at the position $\mathbf{x}'$, the exact location (inside the target cell k) at which an atom was exhibited in configuration i. $Z^+(k,\mathbf{x}')$ thus covers a portion of the total configurational volume spanned by $Z^+(k)$. TP_k for an occupied cell is the probability density, $Z^+(k,\mathbf{x}')/\{[Z^+(k)+Z^-(k)]\}$. After cell k has been treated it becomes a past cell, empty or occupied according to configuration i. For a periodic system, this means that the images of cell k are also becoming part of the fixed past and will thus affect the TPs of the L^3-k remaining future cells. In this HS procedure all the L^3 TPs are calculated *exactly* and their product leads *exactly* to $\rho(\mathbf{x}^N)$ [Eq. (25)]. However, in practice scanning the entire conformational space in order to systematically calculate the exact future partition functions is unfeasible. (The computational time grows exponentially with the number of particles considered, and the number of the grid points used to approximate the continuum.) Therefore we refer to this procedure as the *ideal* HS method.

H. Transition probabilities of the HSMC method

Because the ideal HS method is unfeasible, we have developed an HSMC approach, where instead of calculating exact future partition functions, the future atoms are simulated at each step by MC and the TPs are obtained from the number of counts of atoms in the target cell. Initially, approximate boundary conditions were used and only part of the future was treated.[9] More recently, however,[18] the HSMC method was developed so as to include the entire future at each HS step (i.e., all the future atoms are simulated by MC) and the periodic boundary conditions are taken into account as well. (It was termed ''complete HSMC'' in Ref. 18, but is presently referred to as simply HSMC.) This method (studied here) is capable, in principle, of yielding the *ideal* HS result (described above) in the limit of infinite future MC sampling. For finite sampling, HSMC provides approximations P_i^{HS} for the Boltzmann probability P_i^B, which improve as the sampling is increased, thus giving rise to narrowing rigorous bounds for F and S (e.g., S^A, F^A, and F^B) as discussed earlier.

HSMC is conducted as follows. At step k, the previously defined N_k atoms, as well as their associated images, are held fixed in their assigned positions (in configuration i), while all the remaining $N-N_k$ future atoms are allowed to move. An MC trajectory is generated for the $N-N_k$ future atoms, and the TP is determined from atom counts in the target cell k. The simulation is performed under standard periodic rules, with the exception that regions inside previously defined cells are excluded. Any trial move that would place a future

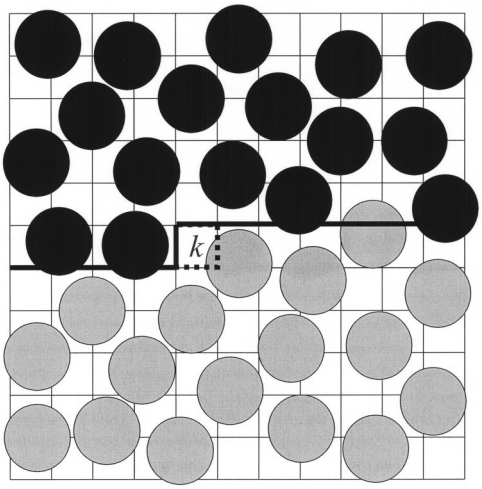

FIG. 1. A two-dimensional (2D) illustration of the main simulation box at the kth step of the HSMC reconstruction. The 2D ''volume'' is divided into cells, where $k-1$ of them have already been considered in previous steps (starting from the upper left corner). These $k-1$ cells comprise the ''past volume'' (the region above the heavy lines) which contains previously treated fixed atoms that are denoted by full black circles defined by the van der Waals radius. This region is excluded from the moveable future atoms (denoted by full gray circles) which are thus simulated in the ''future volume'' below the heavy lines, while in the presence of the fixed atoms. The future atoms can visit the target cell k (depicted by dotted lines) and their counts in this cell lead to the transition probability of an empty cell or the transition probability density of an occupied one. Note that for the case of an occupied target cell, counts are actually accumulated for visitations to a smaller region, V_{cube} (see text), located inside the target cell but not shown in the figure.

atom into this previously assigned volume is rejected. A two-dimensional representation of the main simulation box is given in Fig. 1. It is evident that as this treatment proceeds the number of moveable future atoms decreases, and the fully mobile system at the beginning becomes gradually ''frozen down'' into the exact configuration i.

The transition probabilities are calculated (from the counts) in the following way. We denote by M_{tot} the total number of attempted moves in the MC simulation for any reconstruction step k. M_{cell} is the number of counts for which an atom was observed in the target cell k. The probability for the target cell to be occupied (unoccupied) by an atom is thus given by

$$P_{\text{occ}}=\frac{M_{\text{cell}}}{M_{\text{tot}}} \quad \text{and} \quad P_{\text{unocc}}=1-P_{\text{occ}}. \tag{29}$$

For the case where the target cell k is vacant in configuration i, the transition probability is $\text{TP}_k=P_{\text{unocc}}$. For an occupied target cell, one has to calculate the probability density ρ_{occ} for an atom to be located at the precise location (inside cell k) at which it is found in configuration i. For this we define a much smaller volume (inside cell k), termed a ''cube,'' which is centered at the exact atom position (in configuration i). We count the visitations of atoms within this cube during the MC simulation and thus estimate the probability density as

$$\rho_{\text{occ}}=P_{\text{occ}}\left(\frac{M_{\text{cube}}}{M_{\text{cell}}}\right)\left(\frac{1}{V_{\text{cube}}}\right)=\left(\frac{M_{\text{cube}}}{M_{\text{tot}}}\right)\left(\frac{1}{V_{\text{cube}}}\right), \tag{30}$$

where M_{cube} is the number of cube counts and V_{cube} is the cube volume. For occupied target cells $\text{TP}_k=\rho_{\text{occ}}$. Note, however, that the probability density is assumed to be uniform over the cube volume. To increase the quality of the results, we actually scale ρ_{occ} by an ensemble averaged weighting factor (see below), which serves to measure the probability density at the atom position more accurately.

The total product of TP_k over all L^3 cells—a product of N transition probability densities ρ_{occ} and L^3-N transition probabilities for empty cells, gives rise to the estimate $\rho^{\text{HS}}(\mathbf{x}^N)$ for the Boltzmann probability density $\rho(\mathbf{x}^N)$,

$$\prod_k \text{TP}_k=N!\rho^{\text{HS}}(\mathbf{x}^N)\approx N!\,\frac{\exp[-E(\mathbf{x}^N)/k_BT]}{Z_N}. \tag{31}$$

Notice that the counting procedure (for the TP_k) does not distinguish between labeled atoms, while in the integration leading to Z_N all the labeled arrangements contribute, hence $\rho(\mathbf{x}^N)$ [Eqs. (25)–(27)] is a labeled probability density, and $N!$ is required in Eq. (31).

I. Implementation details and enhancements of the method

Several enhancements to the HSMC method have been implemented. One of which is MC preferential sampling,[28–31] which imposes more frequent trial moves for atoms which are close to the target cell. In our implementations the trial probability of each atom is proportional to $1/r^2$, where r is the atom's distance measured from the center of the target cell. To keep the trial probability from becoming arbitrarily large at small r, the weighting becomes flat for r^2 less than ~ 3 Å^2. Additionally, it is beneficial to allow the number of MC steps at each cell (M_{tot}) to decrease (on average) as the number of future atoms decreases (i.e., with increasing k). In particular, we allow the *maximum* (see below) number of steps to depend linearly on the number of future molecules (until there are fewer than 20, in which case it is constant). Furthermore, the total MC run length for any particular target cell is also based on its estimated sampling difficulty, which is determined from preliminary cube/cell counts accumulated during the equilibration period. In other words, more steps are given to cells that would be expected to have low transition probabilities. If, for example, very few cube counts (occupied cell) are accumulated during the equilibration period, then the maximum number of steps is performed in the production run. Otherwise, for cases of higher preliminary counts, the run length is shorter (scaled down). There are many ways to carry out this weighting. We use several empirical settings (discrete categories) through which the number of steps is reduced from the maximum number (by up to a factor of about 5 or 10). We further suggest treating occupied and unoccupied cells separately. As the unoccupied cells tend to be far easier to count reliably, significantly fewer steps should be allotted to them on average. Additional discussion of the above topics is available in Ref. 9.

Another important modification is the ensemble averaged weighting factor (mentioned above), which gives more accurate transition probability densities. This is computed

TABLE I. The systems studied and the standard MC and HSMC running conditions. N is the number of molecules, T is the temperature, and E is the average potential energy. Other parameters are explained in the text.

N	Density[a]	T (K)	$-E$[b]	Box length (Å)	Cell length (Å)	Cube length (Å)
			Argon			
32	0.846	96.53	6.063(1)	11.4293	2.2859	0.3810[c]
64	0.846	96.53	5.9844(3)	14.4	2.40	0.3429[c]
125	0.846	96.53	5.9883(3)	18.0	2.25	0.3750[c]
			Water			
64	1.000	298.15	9.987 (2)	12.418	2.0697	0.2957,[d] 0.6899[e]

[a]Density for argon is given as the reduced density $\rho^* = N\sigma^3/V$, where V is the volume and σ is the Lennard-Jones distance parameter. Density for water is given in g/cm^3.

[b]The potential energy E for argon is given in reduced units, $E^*/N = E/\epsilon N$, where ϵ is the Lennard-Jones energy parameter. For water, the potential energy is in kcal/mol. The statistical error (for E) appears in parentheses; for example, 5.9844 (3)=5.9844±0.0003.

[c]We have used a convention such that (cube length)=(cell length)/J, where J is an integer ($J=6$, 7, and 6 for $N=32$, 64, and 125, respectively); therefore, the cube lengths for the three argon systems are slightly different. However, this convention is unnecessary, and all three systems could have been run at any one of these cube lengths yielding negligible differences in performance compared to the current results.

[d]Cube length used for the case of ''one-stage sampling,'' where additionally, counts for ρ_{occ} also require the molecular orientation to be in an angular volume of $0.0125\pi^2$ (see text). These Cartesian and angular values were also used in ''two-stage sampling'' to define the smaller cube.

[e]Length of the larger cube (cube°) used in two-stage sampling, where the corresponding (larger) angular volume was $0.1714\pi^2$.

during the HSMC simulation (for an occupied cell) in the following way. Every time an atom is found in the cube (defined above), we calculate the resulting (hypothetical) potential energy for this atom to be repositioned at $\mathbf{x}'$, which is the exact location (inside the cube) at which an atom was exhibited in configuration being analyzed; this is done keeping all other atoms fixed. We denote this energy as $E(\mathbf{x}';\mathbf{x}^{N-1})$ and compare it to $E(\mathbf{x}^N)$, the actual ''undisplaced'' potential energy of the system (as it was found in the HSMC simulation), where it is recognized that the only difference between these two energies is due to the pairs involving the atom to be displaced. The ensemble average $\langle \exp\{-[E(\mathbf{x}';\mathbf{x}^{N-1})-E(\mathbf{x}^N)]/k_BT\}\rangle_{\text{cube}}$ is computed over all cases (during the HSMC simulation) where an atom is found (anywhere) in the cube. The transition probability density [compare with Eq. (30)] is then calculated as

$$\rho_{\text{occ}} = \left(\frac{M_{\text{cube}}}{M_{\text{tot}}}\right)\left(\frac{1}{V_{\text{cube}}}\right) \times \langle \exp\{-[E(\mathbf{x}';\mathbf{x}^{N-1})-E(\mathbf{x}^N)]/k_BT\}\rangle_{\text{cube}}. \quad (32)$$

Typical values for the ensemble average (in brackets) are on the order of 1. Nevertheless, these scaled corrections improve the overall results significantly. A detailed derivation of the weighting factor is given in the Appendix of Ref. 9.

J. The choice of V_{cube}

Provided that the ensemble averaged weighting factor is used, implementations with different values for V_{cube} will always yield the correct free energy F in the limit of very long runs. However, for finite length runs the quality of the free energy bound F^A is affected by the size of V_{cube}. Generally, the ensemble averaged weighting factor (which is a function of cube size) will converge more readily as V_{cube} is made smaller, but a cube that is too small will lead to statistically unreliable cube counts. Thus, cube sizes at either extreme (too large or too small) will give rise to higher fluctuations and lower (poorer) values of F^A.

The following points should be considered when choosing V_{cube}. The probability density is most sensitive to repulsive van der Waals overlaps; therefore, V_{cube} should be small on a scale of the molecular size. Still, a considerable range of V_{cube} values can give acceptable performance. For example, defining $V_{\text{vdW}}=(4/3)\pi(\sigma/2)^3$ as the molecular size of argon, we have found that values of $V_{\text{cube}}/V_{\text{vdW}}$ ranging from 5×10^{-5} to 1×10^{-2} work reasonably well. Though we have not done a systematic optimization, the results reported in this work were generated using $V_{\text{cube}}/V_{\text{vdW}}$ values of about 2×10^{-3} (see Table I). We also used about the same value of $V_{\text{cube}}/V_{\text{vdW}}$ for TIP3P water (V_{cube}, in this context, would actually be denoted by V_{Cart} for water, see Sec. II K below). Here, one can adopt the Lennard-Jones σ value of oxygen or the first peak in the oxygen-oxygen radial distribution function as an approximate molecular diameter. Similar considerations can be used for other molecules.

K. Modifications for water

The implementation described above for argon can be straightforwardly adapted for water. The only fundamental difference is that the molecular orientations must also be taken into account. We take the oxygen as the ''center'' of the molecule and thus determine P_{occ} and P_{unocc} as described earlier. For the transition probability densities, however, we must alter the meaning of V_{cube} in Eq. (30). Thus, we define $V_{\text{cube}}=V_{\text{Cart}}V_{\text{ang}}$, where V_{Cart} as before is a small Cartesian cube and V_{ang} is a small orientational region (i.e., a small portion of the total $8\pi^2$ molecular angular volume). These Cartesian and angular regions are centered on the exact po-

sition and orientation of the actual water molecule in configuration *i*. Thus in the MC simulation, a (future) water molecule will be located in this "molecular cube" whenever its oxygen is located within the specified Cartesian cube V_{Cart} and, simultaneously, the molecular orientation lies in the specified region of angular volume V_{ang}. With these counts, the transition probability density ρ_{occ} can be computed using Eq. (30) where the above "molecular cube" V_{cube} is used. As for argon, one can show that the ensemble averaged weighting factor can be used to increase the accuracy of the probability density. Thus in practice, ρ_{occ} is computed according to Eq. (32), where again $V_{\mathrm{cube}}=V_{\mathrm{Cart}}V_{\mathrm{ang}}$, and molecules located in the (molecular) cube are hypothetically repositioned at $\mathbf{x}'$, which now means the exact Cartesian position *and* orientation at which the molecule was found in the configuration being analyzed. Though the efficiency of the method does depend on the treatment of V_{ang}, we have found, as for the case of V_{Cart}, that acceptable performance can be obtained over a reasonably wide range of specifications. $V_{\mathrm{ang}}=0.0125\pi^2$ in this work is approximately 0.2% of the total molecular angular volume, $8\pi^2$ (see Table I).

L. Two-stage sampling

One of the key challenges in the implementation of the HSMC method for water is the statistical reliability of the counts. This is seen by considering that a water molecule (as treated in most of the common rigid models) has three more degrees of freedom compared to the simple atomic argon; we have found that cube count probabilities (for occupied cells) are typically two or three orders of magnitude smaller for water than for argon. We will thus focus here on the probability for cube counts, denoted explicitly as

$$P_{\mathrm{cube}}=\left\langle \frac{M_{\mathrm{cube}}}{M_{\mathrm{tot}}}\right\rangle, \tag{33}$$

where a "cube count," for the case of water, means being in the molecular cube (described above) where both Cartesian and orientational tolerances are satisfied.

In order to overcome statistical problems associated with very small P_{cube} values, it can be advantageous to break the counting process into two stages. For example, given that a direct (one-stage) determination would be allotted a total simulation length of M_{tot} total steps, these resources could be used for two simulations ("stage 1" and "stage 2") of lengths, $M_{\mathrm{tot}}^{(1)}$ and $M_{\mathrm{tot}}^{(2)}$ (i.e., $M_{\mathrm{tot}}^{(1)}+M_{\mathrm{tot}}^{(2)}=M_{\mathrm{tot}}$). In these simulations we introduce a new volume region, cube°. This region of Cartesian and (for water) angular volume is larger than, and completely contains, the original (smaller) cube.

In the first simulation, stage 1, the HSMC implementation is unaltered except that now counts, $M_{\mathrm{cube}^\circ}^{(1)}$, are determined for the larger cube° and the corresponding probability P_{cube° is calculated, $P_{\mathrm{cube}^\circ}=M_{\mathrm{cube}^\circ}^{(1)}/M_{\mathrm{tot}}^{(1)}$. In the second simulation, stage 2, a molecule is constrained to the region, cube° (but is otherwise mobile). This is done by rejecting any MC move that would cause its coordinates to fall outside the specified Cartesian or angular volume of cube°. Counts, $M_{\mathrm{cube}}^{(2)}$, are now recorded for this molecule to be in the (smaller) cube. With these counts one can calculate the conditional probability for a molecule to be located in the cube given that it is in cube°, $P(\mathrm{cube}|\mathrm{cube}^\circ)=M_{\mathrm{cube}}^{(2)}/M_{\mathrm{tot}}^{(2)}$. The quantity of interest, P_{cube}, [Eq. (33)] can therefore be calculated from this two-stage process as $P_{\mathrm{cube}}=P_{\mathrm{cube}^\circ}\times P(\mathrm{cube}|\mathrm{cube}^\circ)$ and the transition probability density ρ_{occ} would thus be approximated by dividing this quantity by V_{cube}. In practice the weighting factor is used, and ρ_{occ} is thus calculated [compare to Eq. (32)] as

$$\rho_{\mathrm{occ}}=\left\langle \frac{M_{\mathrm{cube}^\circ}^{(1)}}{M_{\mathrm{tot}}^{(1)}}\right\rangle\left\langle \frac{M_{\mathrm{cube}}^{(2)}}{M_{\mathrm{tot}}^{(2)}}\right\rangle\left\langle \frac{1}{V_{\mathrm{cube}}}\right\rangle \times\langle \exp\{-[E(\mathbf{x}';\mathbf{x}^{N-1})-E(\mathbf{x}^N)]/k_BT\}\rangle_{\mathrm{cube}}, \tag{34}$$

where the ensemble average is accumulated (during stage 2) over all cases where the molecule is found in the (smaller) cube.

The logic behind this procedure is that when the cube counting probabilities P_{cube} become very small, it can be more reliable to alternatively measure the two probabilities P_{cube° and $P(\mathrm{cube}|\mathrm{cube}^\circ)$, which are far larger than P_{cube}, even if they are measured with shorter simulations. We have applied two-stage sampling (for water) to all occupied cells (no modifications are made for the empty cells). In our implementations, stage 1 and stage 2 are run to the same number of MC steps ($M_{\mathrm{tot}}^{(1)}=M_{\mathrm{tot}}^{(2)}$). The volumes defining the (smaller) cube are as given in the preceding section. (i.e., they are the same as is used in the one-stage implementation.) For cube°, we have taken Cartesian and angular volumes that are roughly 13 and 14 times larger than their corresponding cube values, respectively. (Better choices are likely to exist as we have not systematically optimized these values.) Two-stage sampling has indeed provided a substantial increase in efficiency when it is applied to water. (For example, comparing cases in which ($M_{\mathrm{tot}}^{(1)}+M_{\mathrm{tot}}^{(2)}$) is equivalent to M_{tot} for one-stage.) Argon on the other hand, which (on average) exhibits much higher values for P_{cube}, shows no significant improvement for the running conditions that we tried.

M. Stochastic probabilities and the bounds for *S* and *F*

The theory developed in Secs. II A–II E is based on deterministic probabilities, while those defined by HSMC are stochastic bearing some noise. In the Appendix we rigorously prove that all the theoretical conclusions of these sections also apply to HSMC, in particular, S^A is an upper bound, F^A is a lower bound, F^B and F_{G}^B are upper bounds, and F^D is exact.

The noise in the HSMC probabilities results from statistical noise in the counts for the transition probabilities. It is actually fundamental in its effects on the free energy and entropy estimates. The shorter the HSMC simulations (small M_{tot}), the greater the noise in the probabilities, and as shown in the Appendix, this effect manifests itself in an average sense by overestimating the entropy (i.e., S^A) and underestimating the free energy (i.e., F^A). We note further that the effect of stochastic probabilities, and subsequent noise in the resulting $F_i^{\mathrm{HS}}(=[E_i+k_BT\ln P_i^{\mathrm{HS}}])$ values, implies an appro-

priateness for the Gaussian approximation for F_{G}^{B}, a condition that would not necessarily be expected for general deterministic cases.

It should also be noted that it is possible to compute lower and upper bounds to the free energy by repeated application of the HSMC method to a single configuration. This is unlike previous HS and LS applications where there would be only one value for $F_i^{\mathrm{HS}}=[E_i+k_BT\ln P_i^{\mathrm{HS}}]$. The derivations for the "single configuration" analogs of F^A, F^B, and F^D are available in the Appendix and results are provided in the following section for some selected argon configurations, which support the theoretical predictions. We note that while this single configuration approach can be applied directly for the free energy (due to its zero fluctuation property), it cannot be used to compute the entropy through ensemble average forms related to Eq. (3). However, given that one can obtain, for example, a lower free energy bound F^A with a single configuration, an upper bound for the entropy is defined through the quantity, $(\langle E\rangle - F^A)/T$, using the average energy which is commonly available from the simulation results.

III. RESULTS AND DISCUSSION

The argon systems are comprised of 32, 64, and 125 atoms at $T=96.53\,\mathrm{K}$ and reduced density, $\rho^*=N\sigma^3/V=0.846$. In all cases the interactions were spherically truncated at a distance equal to half the box length, and the long-range energy (tail) corrections were added to the results.[28] The water system consists of 64 TIP3P water molecules[19] at density 1.000 g/cm^3 and temperature $T=298.15\,\mathrm{K}$. Here molecule-based spherical truncation was applied (again, at half the box length) but no long-range correction was added. The details of the MC and HSMC running conditions are summarized in Table I. Also provided in this table are the average potential energies for each system, which were determined from the Monte Carlo simulations described below. For brevity we do not report entropy values directly; however, these energies along with the free energies reported in following tables make the corresponding entropies available.

The sample configurations (which are analyzed in the HSMC procedure) were generated using the usual Metropolis MC simulation method[5] in the NVT ensemble under standard periodic boundary conditions. Thus, at each MC step an atom (molecule) is selected at random and a random translational trial move is generated within a small Cartesian cube around the atom position. For water, the molecule is also given a small (random) rotation about a randomly chosen axis. Cartesian and rotational step sizes were chosen to give ~40%–50% acceptance. Configurations were recorded at long enough intervals to give an uncorrelated sample. The MC simulations of the future molecules during the HS reconstruction process are very similar to the standard MC simulations. The exceptions (which were discussed above) are: the system is only partially mobile, the moveable future atoms (molecules) are excluded from the previously treated regions, and atoms (molecules) are selected preferentially for trial moves based on their proximity to the target cell. Additionally, the number of MC steps at each cell, M_{tot}, was not constant but varied with the number of future molecules and other criteria outlined in Sec. II I. The results (Tables II, IV, and V and Figs. 2 and 3) are therefore given as a function of the *average* number of MC steps per cell, denoted $\bar{M}_{\mathrm{tot}}$. In the case of two-stage sampling, we take the number of MC steps (for any occupied cell) as the total of the two simulations (stages), and therefore the reported $\bar{M}_{\mathrm{tot}}$ includes all computational investment (all MC steps taken), thus allowing straightforward comparison with the one-stage procedure. [Here, whenever M_{tot} is the same (for one- and two-stage), each simulation in the two-stage procedure is run half

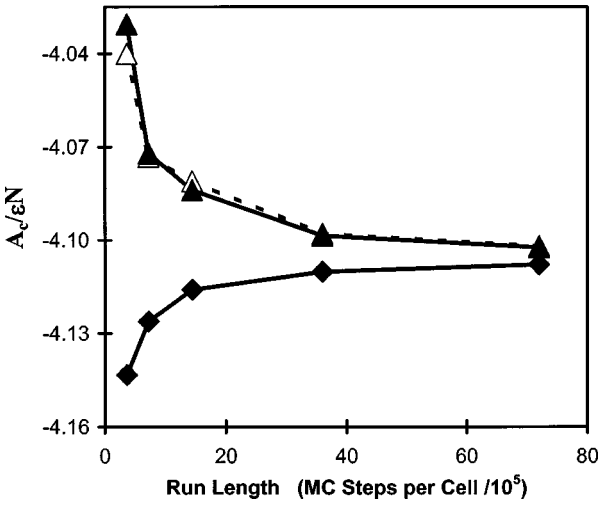

FIG. 2. Free energy bounds as a function of HSMC run length for argon, $N=32$ atoms. The HSMC run length on the horizontal axis is given as $\bar{M}_{\mathrm{tot}}$, the average number of MC steps per cell. Shown are the free energy lower bound F^A (diamonds and solid lines), the upper bound F^B (open triangles and dashed lines), and the Gaussian upper bound F_{G}^{B} (solid triangles and solid lines). Free energies are given as $A_c/\epsilon N$, where A_c is the configurational free energy defined in Eq. (28), ϵ is the standard Lennard-Jones energy parameter, and N is the number of atoms.

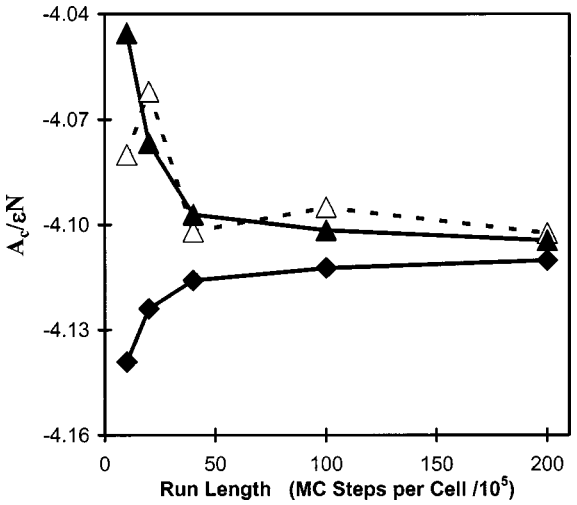

FIG. 3. Free energy bounds as a function of HSMC run length for argon, $N=125$ atoms. The HSMC run length on the horizontal axis is given as $\bar{M}_{\mathrm{tot}}$, the average number of MC steps per cell. For details, see the caption of Fig. 2.

TABLE II. HSMC results for argon. Free energy values are given as $A_c/\epsilon N$, where A_c is the configurational free energy [Eq. (28)], ϵ is the standard Lennard-Jones energy parameter, and N is the number of atoms. F^A [Eq. (6)] is a lower bound of the free energy and σ_A [Eq. (7)] is its fluctuation. F^B [Eqs. (8) and (9)] is an upper bound and F_G^B [Eq. (17)] is its corresponding Gaussian approximation. F^M [Eq. (12)] and F_G^M [Eq. (18)] are the averages of F^A with F^B and F_G^B, respectively. F^D [Eq. (20)] is the direct estimate for the free energy. R is the acceptance rate for the reversed-Schmidt procedure [Eq. (11)] and R_G is the corresponding Gaussian result (see text). $\overline{M}_{tot}$ is the average number of MC steps per cell. n is the number of configurations analyzed (the sample size), where a single HSMC reconstruction was performed on each configuration. Results obtained by thermodynamic integration are denoted as TI. The statistical error appears in parenthesis; for example, 4.108(1)=4.108±0.001. F^A and σ_A are reported here as *per molecule* quantities; however, Eq. (17) as written for F_G^B requires these quantities to be for the system *as a whole*. [This follows, for example, from Eq. (9), which requires the system's probability, as a whole.] Thus the values given here must be multiplied by N before using Eqs. (17) and (18) for F_G^B and F_G^M, respectively.

$\overline{M}_{tot}$	$-F^A$	σ_A	$-F^B$	$-F_G^B$	$-F^M$	$-F_G^M$	$-F^D$	R	R_G	n
				$N=32$						
360 000	4.143 (1)	0.0533(5)	4.040(4)	4.030 (2)	4.092(4)	4.087 (2)	4.093 (3)	0.13	0.13	2205
720 000	4.1260(8)	0.0369(5)	4.073(4)	4.072 (2)	4.100(4)	4.099 (1)	4.100 (3)	0.31	0.30	2001
1 440 000	4.1159(8)	0.0284(5)	4.081(3)	4.084 (1)	4.098(3)	4.100 (1)	4.099 (2)	0.42	0.43	1410
3 600 000	4.1102(5)	0.0171(5)	4.098(2)	4.0986(8)	4.104(2)	4.1044(6)	4.104 (1)	0.63	0.63	1128
7 200 000	4.1079(4)	0.0117(3)	4.102(1)	4.1024(5)	4.105(1)	4.1051(4)	4.105 (1)	0.74	0.74	725
14 400 000	4.1076(4)	0.0092(3)	4.104(1)	4.1042(5)	4.106(1)	4.1059(4)	4.1058(5)	0.83	0.80	602
TI	4.105 (1)		4.105(1)	4.105 (1)	4.105(1)	4.105 (1)	4.105 (1)			
				$N=64$						
720 000	4.132 (1)	0.0330(5)	4.064(4)	4.046 (3)	4.098(4)	4.089 (2)	4.096 (3)	0.11	0.06	581
1 440 000	4.117 (1)	0.0224(5)	4.079(4)	4.077 (2)	4.098(4)	4.097 (1)	4.098 (3)	0.19	0.21	495
2 880 000	4.1085(8)	0.0167(5)	4.087(3)	4.086 (2)	4.098(3)	4.097 (1)	4.097 (2)	0.38	0.35	459
7 200 000	4.1046(5)	0.0105(5)	4.096(2)	4.096 (1)	4.100(2)	4.1002(7)	4.100 (1)	0.53	0.55	371
14 400 000	4.1025(5)	0.0078(3)	4.097(1)	4.0976(6)	4.100(1)	4.1001(5)	4.1000(8)	0.60	0.66	244
28 800 000	4.1019(4)	0.0053(5)	4.099(1)	4.0997(6)	4.100(1)	4.1008(5)	4.1007(8)	0.76	0.77	174
TI	4.100 (1)		4.100(1)	4.100 (1)	4.100(1)	4.100 (1)	4.100 (1)			
				$N=125$						
1 000 000	4.139 (1)	0.0246(5)	4.08 (2)	4.045 (4)	4.11 (2)	4.092 (2)	4.10 (1)	0.08	0.007	362
2 000 000	4.124 (1)	0.0175(6)	4.06 (2)	4.077 (4)	4.09 (2)	4.100 (2)	4.09 (1)	0.06	0.05	179
4 000 000	4.116 (1)	0.0110(9)	4.10 (1)	4.097 (3)	4.11 (1)	4.107 (2)	4.108 (7)	0.31	0.23	125
10 000 000	4.1124(6)	0.0083(5)	4.10 (1)	4.102 (1)	4.10 (1)	4.1070(9)	4.105 (6)	0.36	0.34	170
20 000 000	4.1102(6)	0.0060(5)	4.10 (1)	4.105 (1)	4.11 (1)	4.1074(8)	4.107 (4)	0.43	0.46	99
TI	4.108 (1)		4.108(1)	4.108 (1)	4.108(1)	4.108 (1)	4.108 (1)			

as long as the corresponding one-stage simulation.] Typically, a *single* HSMC reconstruction is performed on each sample configuration, and the overall results are determined by averaging over a total sample size of n configurations. [See also the description following Eq. (A8) in the Appendix.] An exception is the case in Table IV, where the results are averages for a single configuration which is reconstructed many times.

Several studies of the free energy of argon[24,26,27,32–36] and water[37–43] have been published, most of them for systems that differ in size (as well as other modeling details) from the present ones. Therefore, for an objective evaluation of our results, we also calculated the free energies for our particular systems of argon and water using TI. The Lennard-Jones (LJ) interactions (for both argon and water) were scaled using the shifted scaling potential of Zacharias *et al.*[44] The Coulombic interactions (of water) were also distance-shifted in a similar way; this circumvents possible charge overlap problems, and thus all interactions (LJ and Coulombic) could be ''grown in'' simultaneously. A more detailed description of the TI calculations is available in Ref. 8.

A. Results for argon

Results for the three argon systems ($N=32$, 64, and 125) are provided in Table II. Here the free energy estimates F^A, F^B, F_G^B, F^M, F_G^M, and F^D are reported along with results obtained by TI, which are considered to be exact. All values correspond to the configurational free energy, A_c, defined in Eq. (28). The free energy estimates are given as a function of the average number of MC steps per cell, $\overline{M}_{tot}$, which effectively defines the level of approximation (α); the larger is $\overline{M}_{tot}$ the better the approximation. The expected trends are clearly shown for the lower bound, F^A [Eq. (6)], where the values steadily increase (improve), and approach convergence as $\overline{M}_{tot}$ is increased. For $N=64$, the largest $\overline{M}_{tot}$ leads to a result for the free energy which deviates from the TI value by less than 0.05%. (The statistical error in the TI result is ~0.02%.) The worst approximation, based on 40 times smaller $\overline{M}_{tot}$ still leads to a free energy estimate that is only ~0.8% lower than the TI value. Similar trends in F^A are exhibited for $N=32$ and 125, with the best values deviating by only 0.06% and 0.05%, respectively.

Also provided in Table II are values for σ_A [Eq. (7)], the fluctuation in F^A. As expected, the free energy fluctuations decrease systematically as the approximation improves (i.e., σ_A tends toward zero as F^A approaches the correct value). The smallest σ_A values, 0.0092, 0.0053, and 0.0060, for $N=32$, 64, and 125, respectively are smaller by a factor of 19.1, 19.4, and 12.5 than their energy counterparts, 0.175, 0.103, and 0.075. In general, these expected trends in the fluctuations reflect the reliability of the various free energy

estimates. Moreover, σ_A is used directly in the calculation of F_G^B (and F_G^M) and in the free energy extrapolations (discussed below).

We now discuss the results for the free energy upper bound F^B [Eqs. (8), (9), and (13)]. For the argon systems of $N=32$ and 64, these results (Table II) are considered to be excellent. Statistical reliability is evidenced by the high R values (also in Table II) for the Schmidt acceptance rate [Eq. (11)] in conjunction with the relatively large number of configurations (n) in the samples. Indeed, the upper bound (F^B) consistently decreases (improves) as the approximation improves ($\bar{M}_{\text{tot}}$ increases), giving a smooth trend approaching the correct free energy. The F^B values for the best approximations are in agreement with the TI results within the statistical error. The error values are, however, somewhat higher than those for the lower bound F^A.

It is important to note that for the cases $N=32$ and 64, F^B is in excellent agreement with the new Gaussian upper bound estimate, F_G^B [Eq. (17)]. Differences between the two values are smaller than the statistical uncertainties in all cases except for the smallest $\bar{M}_{\text{tot}}$ for each system. This agreement is also shown in Fig. 2 where F^B, F_G^B, and F^A are given as a function of run length $\bar{M}_{\text{tot}}$ for $N=32$; the difference in the trend lines for F^B and F_G^B is barely visible. These upper bounds along with the lower bound F^A show a clear tightening as the approximation improves. Agreement of F^B and its Gaussian estimate F_G^B is further enforced by noting the similarity of R to the corresponding quantity, R_G (also in Table II). R_G is the hypothetical Schmidt acceptance rate, which is calculated from a Gaussian sample with average F^A and σ_A. The (hypothetical) samples are created using a Gaussian random number generator and thus are far larger than the actual sample sizes analyzed (n), therefore the values can be considered to be exact (actually, more converged than R) within the Gaussian approximation. We note finally that the appropriateness of the Gaussian assumption (in deriving F_G^B) was verified directly by histogramming the F_i^{HS} values, and indeed we have found these results to fit well to a Gaussian distribution within the statistical noise.

For the argon system of $N=125$, F^B is in all cases higher than the correct free energy. Therefore, in this sense, the values are consistent with upper bound estimation. However, the statistical uncertainties are high, and there is no longer a monotone decreasing trend as the approximation improves. As discussed in the theory section, the determination of F^B can become problematic as the system becomes larger, and this, coupled with smaller sample sizes (n), makes F^B less statistically reliable for $N=125$ than it is for $N=32$ and 64. F_G^B, on the other hand, is not as affected by these limitations, as the quantities F^A and σ_A (upon which it depends) are more readily estimated. Indeed, the results for F_G^B are very encouraging; they are much better than F^B (for $N=125$), which is clearly shown in Fig. 3. (Note how F_G^B traces a smooth curve through the more jagged trends in F^B.) Here again, we also see a consistent tightening of the upper (F_G^B) and lower (F^A) bounds as the approximation improves.

Some of the best estimates for the free energy in Table II are provided by F^M [Eq. (12)] and F_G^M [Eq. (18)], which are the averages of the lower bound F^A with the upper bounds F^B and F_G^B respectively. In fact, for each argon system (each N), the best three approximations lead to values of F^M and F_G^M that match the TI value within the statistical uncertainty. For $N=32$ and 64, F^M in all cases provides a better value for the free energy than the corresponding F^A or F^B at the same $\bar{M}_{\text{tot}}$. This is not always true for $N=125$ due to the higher statistical error in F^B. However, given the comparatively robust behavior of F_G^B, it follows that F_G^M provides the most accurate free energy values (compared to F^A, F^B, or F_G^B) at all N and for all $\bar{M}_{\text{tot}}$.

Also impressive are the results for the direct free energy estimate, F^D [Eq. (20)]. As for F^M and F_G^M, the three largest $\bar{M}_{\text{tot}}$ for each N all give F^D values which agree with the TI results within the estimated uncertainty. And again at any given $\bar{M}_{\text{tot}}$, F^D is typically closer to the correct free energy than the corresponding upper and lower bound estimates. As is the case for F^B, the convergence of F^D requires good overlap of the probability distributions P_i^{HS} and P_i^B, but to a lesser extent. The F^D values reach their asymptotic value (as n is increased) more readily than does F^B, and thus the statistical errors are lower. These errors are still higher than for F_G^M, however.

It is important to point out, that of all the free energy estimates discussed, F^A converges by far the fastest (i.e., ''converging'' in the statistical sense, where it approaches its asymptotic lower bound value with increasing n, for any given $\bar{M}_{\text{tot}}$). For this reason, it is stressed that one should always consider in any investigation, the desired accuracy. (That is, how close one needs to be to the exact free energy value for that particular scenario.) If, for example, the desired tolerance were to be within 0.5% of the correct free energy, it is seen that nearly all of the F^A values in Table II are within this range. This implies that in many scenarios, any of these F^A values can be considered to be adequate, and therefore ''correct.'' Furthermore, these F^A values would not change by much if the sample sizes were drastically reduced. As an extreme example, one could treat a single configuration of $N=64$ at $\bar{M}_{\text{tot}}=7\,200\,000$. Given the σ_A value, this configuration would provide the free energy within a small range $[-4.115(-0.35\%),-4.094(+0.15\%)]$ around the correct value -4.100. Or, taking the average of just five configurations, this range would narrow by a factor of 2 and thus produce a value for F^A in the range $[-4.109,-4.100]$. The other free energy estimates are obviously useful when greater accuracy is desired, and furthermore they can provide supporting information (e.g., helping to bracket the correct value) when investigating new systems for which the free energy is unknown. F_G^B is expected to be especially useful in this role, even when the sample sizes are relatively small.

As discussed previously, σ_A must tend toward zero as F^A approaches the correct value. Thus, using the F^A and σ_A results in Table II, extrapolated values for the correct free energy were determined by fitting to the functional form given in Eq. (22). The results are provided in Table III. Data sets were formed using combinations of 3, 4, 5, or 6 (σ_A,F^A) points (all for the same N); any set which resulted

TABLE III. Averages of HSMC extrapolation results for argon. Free energy values are given as $A_c/\epsilon N$, where A_c is the configurational free energy [Eq. (28)], ϵ is the Lennard-Jones energy parameter, and N is the number of atoms. The function $F^A(\sigma_A)$ is approximated from multiple fits (data sets) created from various combinations of (σ_A, F^A) points (approximations) taken from Table II, all for the same N; the results given are averages over all of the data sets. F^{extp} [Eq. (22)] is the extrapolated free energy, F^{up} is an upper bound defined by the tangent of the fit at the best approximation, and F^{M2} is the average of F^{up} with the corresponding F^A value [Eq. (23)]. Results obtained by thermodynamic integration are denoted as TI. The statistical error is defined in the caption of Table II.

N	$-F^{\text{up}}$	$-F^{M2}$	$-F^{\text{extp}}$	F(TI)	Data sets
32	4.1048 (3)	4.1064 (1)	4.1063 (2)	4.105 (1)	29
64	4.0996 (3)	4.1010 (1)	4.1009 (2)	4.100 (1)	28
125	4.1036 (7)	4.1075 (6)	4.1065 (10)	4.108 (1)	10

in a fit that gave positive curvature was discarded. The quantities determined from a data fit are the extrapolated free energy, F^{extp} [Eq. (22)], the tangential upper bound, F^{up} (discussed above), and the average F^{M2} [Eq. (23)]. The results in Table III are the averages of these quantities over all of the data sets (over all fits). For all N, the F^{up} are consistent with upper bound estimation; the values for $N=32$ and 64 are very close to the exact value. F^{M2} and F^{extp} agree with TI within the estimated uncertainty for $N=64$ and 125 (and nearly so for $N=32$), where for all N, F^{M2} was somewhat more precise than F^{extp}. The precision for all quantities was worse for $N=125$ than for 32 and 64, presumably due to the smaller number of data sets.

Provided in Table IV are results obtained from repeated HSMC analysis of the *same* configuration (discussed in Sec. M); given are (the single configuration analogues of) F^A and its fluctuation σ_A, F^B, and F^M. Here, five argon configurations ($N=64$) were investigated, where they are identified using the letters A–E. The selected configurations have energies which are close to the average energy, therefore they all can be considered "typical." The number of trials performed on each of the configurations is also given in the table denoted as "Replications," which is analogous to the sample size n of Table II. Two approximations were studied corresponding to $\overline{M_{\text{tot}}}=720\,000$ and $2\,880\,000$.

It is seen in Table IV that for every configuration (and at both $\overline{M_{\text{tot}}}$) the F^A are consistent with lower bound estimation. However, each individual configuration can give rise to its own distinct F^A value for a given $\overline{M_{\text{tot}}}$. This implies that certain configurations (such as configuration E) will converge to the correct free energy with less computational investment. In other words, results for configuration E can be said to define a better approximation for the same $\overline{M_{\text{tot}}}$. It is important to recognize that these configuration specific variabilities are still relatively small compared to differences observed when $\overline{M_{\text{tot}}}$ is changed. Indeed, the results for the five configurations for $\overline{M_{\text{tot}}}=2\,880\,000$ are far more similar to each other than they are to any of the results for $\overline{M_{\text{tot}}}=720\,000$. This is true as well for the fluctuations σ_A. We note further that the average of F^A for the five configurations is equivalent to the standard HSMC F^A result for both $\overline{M_{\text{tot}}}$.

Similar statements can be made for F^B, where again for all cases it defines an upper bound, the value of which can vary from one configuration to another. Again, the average for the five configurations is similar to the corresponding result from the standard HSMC estimation. We also note that in almost every case the results for F^M provide the best free energy value (compared to the corresponding F^A and F^B). In fact, for $\overline{M_{\text{tot}}}=2\,880\,000$, the F^M values agree with the TI value for all configurations within the statistical uncertainty, and thus show equivalent performance compared to the standard HSMC F^M estimation.

TABLE IV. HSMC results for argon based on single configurations, $N=64$. Free energy values are given as $A_c/\epsilon N$, where A_c is the configurational free energy [Eq. (28)], ϵ is the standard Lennard-Jones energy parameter, and N is the number of atoms. F^A is a lower bound of the free energy [Eq. (A6), analogous to Eq. (6)] and σ_A [defined similar to Eq. (7)] is its fluctuation. F^B [Eq. (A10), analogous to Eqs. (8) and (9)] is an upper bound and F^M is the average of F^A and F^B. $\overline{M_{\text{tot}}}$ is the average number of MC steps per cell. The letters A, B, C, D, and E serve to identify a particular configuration, and "Replications" is the number of times an HSMC result was determined (i.e., the number of reconstructions) for that configuration. The corresponding HSMC results for a given $\overline{M_{\text{tot}}}$ from Table II are denoted as HSMC. Results obtained by thermodynamic integration are denoted as TI. The statistical error is defined in the caption of Table II.

Configuration	$-F^A$	σ_A	$-F^B$	$-F^M$	Replications
		$\overline{M_{\text{tot}}}=720\,000$			
A	4.130 (2)	0.0312 (7)	4.068 (7)	4.099 (7)	211
B	4.141 (2)	0.0285 (7)	4.091 (7)	4.116 (7)	219
C	4.135 (2)	0.0320 (7)	4.080 (7)	4.108 (7)	216
D	4.128 (2)	0.0317 (7)	4.073 (7)	4.100 (7)	219
E	4.128 (1)	0.0278 (5)	4.053 (6)	4.091 (6)	394
HSMC	4.13 (1)	0.0330 (5)	4.064 (4)	4.098 (4)	
TI	4.100 (1)		4.100 (1)	4.100 (1)	
		$\overline{M_{\text{tot}}}=2\,880\,000$			
A	4.106 (1)	0.0168 (6)	4.088 (4)	4.097 (4)	184
B	4.110 (1)	0.0159 (6)	4.092 (4)	4.101 (4)	201
C	4.112 (1)	0.0151 (6)	4.097 (4)	4.104 (4)	172
D	4.111 (1)	0.0145 (6)	4.092 (4)	4.102 (4)	192
E	4.106 (1)	0.0137 (6)	4.091 (4)	4.098 (4)	182
HSMC	4.1085 (8)	0.0167 (5)	4.087 (3)	4.098 (3)	
TI	4.100 (1)		4.100 (1)	4.100 (1)	

B. Results for water

HSMC results are presented for water in Table V, which contains estimates for both the one- and two-stage sampling procedures (see Sec. L). The various free energy estimates (and other quantities) presented are for the most part the same as for Table II. Here all free energies correspond to the excess free energy F_e defined in Eq. (27). Viewing the one- and two-stage results separately, the expected trends in the lower bound, F^A, are again clearly shown. The values for F^A steadily improve (increase) as $\overline{M_{\text{tot}}}$ is increased and the corresponding fluctuations decrease. The best value for F^A, -5.627 kcal/mol, is 0.5% lower than the TI value (-5.599), and here σ_A, 0.024 (kcal/mol), is 7.8 times smaller than the energy fluctuation, 0.187.

The difference in the performance of the one- and two-stage approaches is striking. The two-stage variant appears to be about three times more efficient, where for example, the (two-stage) F^A value at $\overline{M_{\text{tot}}}=5\,312\,000$ is higher (better)

TABLE V. HSMC results for 64 TIP3P water molecules. Free energy values are given as the excess free energy, F_e [Eq. (27)], in units of kcal/mol. F^A [Eq. (6)] is a lower bound of the free energy and σ_A [Eq. (7)] is its fluctuation. F^B [Eqs. (8) and (9)] is an upper bound and F_G^B [Eq. (17)] is its corresponding Gaussian approximation. F_G^M [Eq. (18)] is the average of F^A and F_G^B. F^D [Eq. (20)] is the direct estimate for the free energy. R is the acceptance rate for the reversed-Schmidt procedure [Eq. (11)] and R_G is the corresponding Gaussian result. $\overline{M}_{tot}$ is the average number of MC steps per cell. n is the number of configurations analyzed (the sample size), where a single HSMC reconstruction was performed on each configuration. Results obtained by thermodynamic integration are denoted as TI. The statistical error is defined in the caption of Table II. See also the caption of Table II for details regarding the computation of F_G^B.

$\overline{M}_{tot}$	$-F^A$	σ_A	$-F^B$	$-F_G^B$	$-F_G^M$	$-F^D$	R	R_G	n
				One-stage					
5 312 000	5.90 (2)	0.102(8)	5.67[a]	4.8 (2)	5.34 (9)	5.70	0.08	$<10^{-7}$	48
13 280 000	5.76 (1)	0.066(5)	5.63	5.29 (7)	5.53 (4)	5.66	0.08	$<10^{-6}$	40
26 560 000	5.703(7)	0.042(5)	5.64	5.51 (5)	5.61 (2)	5.66	0.21	0.001	38
TI	5.599(2)		5.599(2)	5.599 (2)	5.599(2)	5.599 (2)			
				Two-stage					
5 312 000	5.736(5)	0.064(5)	5.58	5.29 (7)	5.52 (4)	5.62 (4)	0.06	$<10^{-6}$	147
13 280 000	5.679(4)	0.040(4)	5.61	5.51 (4)	5.59 (2)	5.63 (3)	0.07	0.002	94
26 560 000	5.636(3)	0.027(3)	5.59 (3)	5.555(18)	5.595(9)	5.607(15)	0.16	0.036	100
53 120 000	5.627(3)	0.024(3)	5.57 (3)	5.565(16)	5.596(8)	5.595(15)	0.16	0.067	87
TI	5.599(2)		5.599(2)	5.599 (2)	5.599(2)	5.599 (2)			

[a]Though the values for F^B are reasonably close to the correct free energy, the expected upper bound trends are not exhibited due to lack of convergence and thus no statistical errors are given.

than the one-stage result at $\overline{M}_{tot}=13\,280\,000$. Indeed, all of the F^A values for the two-stage approach are significantly higher, given the same $\overline{M}_{tot}$, and correspondingly, the σ_A are all lower. As discussed in the Theory section, the cube count probabilities for water can be very small (compared to argon) because of the extra orientational allignment which must be observed. The two-stage approach avoids direct measurement of these very small probabilities by, instead, invoking much larger conditional probabilities which are measured using two (shorter) simulations. The results in Table V clearly show this to be advantageous.

While the (two-stage) results for F^A (for water) are very good, better accuracy can be achieved through the utilization of the other free energy estimates. The results for F_G^B are particularly helpful. The expected upper bound behavior is observed as F_G^B consistently decreases (improves) approaching the correct free energy as the approximation improves. Correspondingly, the results for the average estimate F_G^M are excellent, where the best value gives -5.596 kcal/mol (compared to -5.599 for TI or -5.627 using F^A alone). The best three approximations for the two-stage approach all match the TI value within the statistical uncertainty. The one-stage results have also been significantly augmented with the Gaussian estimates, where F_G^M for the best two approximations is far superior to using F^A alone, and the best of these approximations also agrees with TI within the error.

The utility of F_G^B is apparent when compared to the standard upper bound F^B. In the two-stage results, the F^B values successfully provide an upper bound estimate in most cases, however, the uncertainties are high and a monotone decreasing (improving) trend is not observed as $\overline{M}_{tot}$ is increased. The one-stage results are worse due to poorer approximation [of $\rho_i^{HS}(\mathbf{x}^N)$ compared to two-stage] along with smaller sample sizes n. In general, far more sampling (larger n) would be required to improve the results for F^B, a condition which is obviously not necessary for its Gaussian approximation (F_G^B). The need for more configurations in the estimation of the standard F^B is further evidenced by the small R and R_G values for the Schmidt acceptance rate; the lower is R, the more configurations that are necessary. We note further that here, any differences between R and R_G are actually more an artifact of the relatively small sample sizes (compared to what would be required) which are applied in the estimation of F^B. Specifically, if R is to be very small, a small sample will often result in estimates for R which are too high because the reversed-Schmidt sampling scheme has not equilibrated. Recalling that R_G comes from drawing a very large number of (Gaussian) random numbers, it can be considered to be more correct.

Though related to F^B, the direct estimate F^D was shown for argon to converge (to its asymptotic value) more readily, and the same is true here for water. The results for F^D are in fact quite good, where the best two approximations give -5.607 and -5.595 kcal/mol, thus deviating from the TI value (-5.599) by only 0.1%. The F^D values for all of the two-stage approximations agree well with TI, being significantly closer than the corresponding values for the lower bound, F^A, or the upper bound, F_G^B. In general, the one-stage approximations are not good enough to obtain high quality F^D values from small sample sizes. Though the values are closer than the corresponding results for F^A, and therefore can be considered as "useful information," convergence is difficult to judge and larger sample sizes would be necessary.

C. Efficiency of HSMC

At this stage of development the HSMC method is still significantly less efficient than TI. Using the example given above, reconstructing a single argon configuration of $N=64$ and $\overline{M}_{tot}=7\,200\,000$ (which would yield the free energy in a small range $[-4.115,-4.094]$ around the correct value -4.100) requires 3.6 h CPU; the TI run for this system required $\sim 1/3$ of this time. The TIP3P model of water, being more complex than the argon system, requires more sam-

pling and significantly larger computer time for calculating the energy at each MC step. The reconstruction of a single configuration at $M_{\mathrm{tot}}=13\,280\,000$ (which would give the correct free energy within about 1%) requires 24 h CPU, compared to ~6 h for the TI run. However, the HSMC program can still be optimized reducing the computer time significantly. Current work, for example, involves the implementation of ''multistage'' counting approaches and advanced (importance) sampling techniques, such as force bias MC.[45] Furthermore, to increase the general applicability of the method, we are currently replacing the future MC simulations by MD simulations, an implementation that requires changing the HSMC build-up procedure.

IV. CONCLUSIONS

The HS method can be applied to fluids in different approximations, as shown in Refs. 8 and 9, and in an exact manner, as has been demonstrated in Ref. 18 and in this paper. With TI an ideal gas is integrated reversibly by gradually changing the potential energy parameters to their final values. The HSMC method is different: The absolute free energy is obtained, *in principle*, by reconstructing a single configuration, i.e., placing its molecules gradually into their positions using transition probabilities. Therefore, HSMC constitutes a new research tool independent of TI and related methods, which enables one to calculate F by analyzing a *given* MC or MD sample. HSMC is general and can be applied to various systems such as, magnetic (lattice) models, polymers, peptides, and proteins in vacuum and in explicit solvent; hence, the theory developed in this paper is of general applicability as well. Recently, HSMC has been extended to peptides,[20] a project that is being continued. Our goal is to use this method to determine the relative stability (i.e., the difference in the absolute free energy, $\Delta F_{m,n}=F_m-F_n$) of different states n and m of peptides, surface loops, etc., solvated in explicit water, where the calculations are based on two samples only without the need to resort to procedures which are dependent on complex integration paths.

ACKNOWLEDGMENTS

This work was supported by NIH Grant No. R01 GM61916 and by NIH Grant No. R01 GM66090.

APPENDIX: PROPERTIES OF THE ENTROPY AND FREE ENERGY FUNCTIONALS BASED ON STOCHASTIC HSMC PROBABILITIES

In the Theory section we have discussed the properties (inequalities) of several entropy and free energy functionals depending on an approximate but *deterministic* probability distribution P_i^{HS}. Here we prove rigorously that these properties also hold for these functionals defined with the stochastic probabilities of HSMC. For compactness in notation, we will write P_i, instead of P_i^{HS}, for the HSMC probabilities. The HS superscript on the corresponding free energy estimate, $F_i^{\mathrm{HS}}(=E_i+k_BT\ln P_i)$, will however be maintained here.

We first point out that unlike the deterministic case, TP_k calculated at step k of configuration i is a random variable. Thus, one can envisage carrying out many trial runs of length M_{tot}, which give rise to a distribution, $\rho(\alpha;\mathrm{TP}_k)$ of the TP_k values, where $\rho(\alpha;\mathrm{TP}_k)$ is unique to the chosen run length and other HSMC running conditions, denoted collectively by α. Clearly, increasing M_{tot} will narrow the width of the distribution, and we assume that at very large M_{tot}, the correct TP would always be obtained. That is, $\mathrm{TP}_k\rightarrow\mathrm{TP}_k^B$ as $M_{\mathrm{tot}}\rightarrow\infty$, where TP_k^B is the exact Boltzmann TP for the building step k of i. In what follows, a discrete system is considered for simplicity. (The applicability for continuum systems should be apparent.) Therefore, any TP_k is simply given by $\mathrm{TP}_k=M_k/M_{\mathrm{tot}}$, with M_k being the number of times the state of interest was observed in a trial simulation for step k.

We now write formally the expectation value of TP_k, which can be obtained *exactly* from n_{rep} trial simulations (j) of TP_k, each of length M_{tot}, where $n_{\mathrm{rep}}\rightarrow\infty$,

$$\langle \mathrm{TP}_k\rangle_\alpha=\int_0^1(\mathrm{TP}_k)\rho(\alpha;\mathrm{TP}_k)d(\mathrm{TP}_k)$$

$$=\lim_{n_{\mathrm{rep}}\rightarrow\infty}\left[\frac{1}{n_{\mathrm{rep}}}\sum_{j=1}^{n_{\mathrm{rep}}}\mathrm{TP}_{k_j}\right]. \tag{A1}$$

The bracket notation $\langle\ \rangle_\alpha$ (which will be used often here) is subscripted with α to emphasize the particular M_{tot} and other HSMC conditions. It is important to show that $\langle \mathrm{TP}_k\rangle_\alpha$ is equal to TP_k^B;

$$\langle \mathrm{TP}_k\rangle_\alpha=\lim_{n_{\mathrm{rep}}\rightarrow\infty}\left[\frac{1}{n_{\mathrm{rep}}}\sum_{j=1}^{n_{\mathrm{rep}}}\mathrm{TP}_{k_j}\right]$$

$$=\lim_{n_{\mathrm{rep}}\rightarrow\infty}\left[\frac{1}{n_{\mathrm{rep}}}\sum_{j=1}^{n_{\mathrm{rep}}}\frac{M_{k_j}}{M_{\mathrm{tot}}}\right]$$

$$=\lim_{n_{\mathrm{rep}}\rightarrow\infty}\left[\frac{\Sigma_{j=1}^{n_{\mathrm{rep}}}M_{k_j}}{n_{\mathrm{rep}}M_{\mathrm{tot}}}\right]=\mathrm{TP}_k^B. \tag{A2}$$

The latter form is seen as a single simulation, which tends to infinite length, and therefore must give TP_k^B. It is stressed that the result $\langle \mathrm{TP}_k\rangle_\alpha=\mathrm{TP}_k^B$ is true for *any* choice of the parameters, α (e.g., M_{tot}). However, other averages such as $\langle \ln \mathrm{TP}_k\rangle_\alpha$ *do* in general depend on α.

As the TP_k are random variables, the HSMC approximated probability, $P_i=\Pi_k\mathrm{TP}_k$, is also a random variable. Furthermore, because the TP_k are independent (i.e., the outcome for TP_k at k does not depend on the outcome for any other TP_l at l), the expectation value of P_i is equal to the Boltzmann probability P_i^B;

$$\langle P_i\rangle_\alpha=\left\langle\prod_k\ \mathrm{TP}_k\right\rangle_\alpha=\prod_k\ \langle \mathrm{TP}_k\rangle_\alpha=\prod_k\ \mathrm{TP}_k^B=P_i^B. \tag{A3}$$

This result is again independent of the parameter set α.

We now aim to show that the average free energy estimate obtained from repeated HSMC determinations for the same configuration i is a lower bound. The free energy estimate $F_{i_j}^{\mathrm{HS}}$ from any single determination (trial j) is given by $F_{i_j}^{\mathrm{HS}}=E_i+k_BT\ln P_{i_j}$, where E_i is the energy of configuration

i. The expectation value of F_i^{HS} (corresponding to repeated HSMC determinations performed on the same configuration i, and with the running conditions α) is given by

$$\lim_{n_{\mathrm{rep}}\to\infty}\left[\frac{1}{n_{\mathrm{rep}}}\sum_{j=1}^{n_{\mathrm{rep}}} F_{i_j}^{\mathrm{HS}}\right]_\alpha = \langle F_i^{\mathrm{HS}}\rangle_\alpha = E_i + k_B T\langle \ln P_i\rangle_\alpha . \tag{A4}$$

Jensen's inequality[46] states that if x is a random variable, and $f(x)$ is a concave function then $\langle f(x)\rangle \leqslant f(\langle x\rangle)$; if $f(x)$ is convex the inequality is reversed. Applying this to $\ln P_i$, which is a concave function of P_i, and using $\langle P_i\rangle_\alpha = P_i^B$ [Eq. (A3)] we obtain

$$\langle \ln P_i\rangle_\alpha \leqslant \ln(\langle P_i\rangle_\alpha) = \ln P_i^B \tag{A5}$$

Thus, defining $F_i^A = F_i^A(\alpha) = \langle F_i^{\mathrm{HS}}\rangle_\alpha$ we prove

$$F_i^A = \langle F_i^{\mathrm{HS}}\rangle_\alpha = E_i + k_B T\langle \ln P_i\rangle_\alpha \leqslant E_i + k_B T \ln P_i^B = F, \tag{A6}$$

where $F = E_i + k_B T \ln P_i^B$ is the correct free energy. Notice that this relation holds for *any* i and not only for the typical equilibrium configurations for the given ensemble.

We now consider functionals which are defined over the whole ensemble, and thus address stochastic variability of all the P_i. S^A for HSMC is now defined as the expectation value of the deterministic form for S^A in Eq. (5), and using Eq. (A5), it is shown to be an upper bound;

$$S^A = \left\langle -k_B \sum_i P_i^B \ln P_i \right\rangle_\alpha$$

$$= -k_B \sum_i P_i^B \langle \ln P_i\rangle_\alpha \geqslant -k_B \sum_i P_i^B \ln P_i^B = S. \tag{A7}$$

Similarly, F^A, defined for HSMC as the average of Eq. (6), is a lower bound of F;

$$F^A = \left\langle \sum_i P_i^B [E_i + k_B T \ln P_i] \right\rangle_\alpha$$

$$= \sum_i P_i^B (E_i + k_B T\langle \ln P_i\rangle_\alpha) = E - TS^A \leqslant F. \tag{A8}$$

S^A and F^A are averages based on not only the Boltzmann distribution, but also on the distributions, $\rho(\alpha;P_i)$, for all the P_i generated with the HSMC method. In practice, the sampling of these distributions is implicit. That is, a sample configuration i is drawn from the Boltzmann distribution (presumably using MC or MD), and then a *single* value for P_i is drawn from $\rho(\alpha;P_i)$ (implicitly) by analyzing this structure with the HSMC method. This process is repeated, and the accumulated (simple) arithmetic averages of $[-k_B \ln P_i]$ and $[E_i + k_B T \ln P_i]$ thus give estimates for S^A and F^A, respectively. Asymptotically, these averages must approach S^A and F^A exactly, and because the distributions are well peaked about the average E and $\ln P$, estimation is expected to be efficient.

The free energy upper bound F^B [Eq. (8)] is now defined for the case of HSMC as

$$F^B = \left\langle \sum_i P_i (E_i + k_B T \ln P_i) \right\rangle_\alpha$$

$$= \sum_i \langle P_i\rangle_\alpha E_i + k_B T \sum_i \langle P_i \ln P_i\rangle_\alpha$$

$$= E + k_B T \sum_i \langle P_i \ln P_i\rangle_\alpha$$

$$\geqslant E + k_B T \sum_i P_i^B \ln P_i^B = F. \tag{A9}$$

In Eq. (A9) we have used the following relations: because $\langle P_i\rangle_\alpha = P_i^B$, $\Sigma_i \langle P_i\rangle_\alpha E_i$ is the Boltzmann average of the energy E. Also, $P_i \ln P_i$ is a convex function of P_i, therefore using Jensen's inequality we have $\langle P_i \ln P_i\rangle_\alpha \geqslant \langle P_i\rangle_\alpha \ln\langle P_i\rangle_\alpha = P_i^B \ln P_i^B$, which holds for all configurations i; thus we obtain $F^B \geqslant F$. F^B, as defined for HSMC in Eq. (A9), can be estimated (as in the deterministic case) by sampling with P_i^B. Equation (A9) can thus be rewritten in the same form as Eq. (9) [or Eq. (13)], where the numerator and the denominator are now expectation values (averaged over the stochastic P_i). We note further that it is these expectation values that are approximated with a Gaussian form in Eqs. (15) and (16). It is thus more clear that the Gaussian approximation is feasible particularly for HSMC, where ''noise'' is imparted in the F_i^{HS} by the stochastic probabilities.

It is also possible to compute an upper bound to the free energy by averaging over a single configuration. It follows from the development related to Eq. (A9) that we can write $P_i^B E_i + k_B T\langle P_i \ln P_i\rangle_\alpha \geqslant P_i^B E_i + k_B T P_i^B \ln P_i^B$ for any configuration i. Therefore, using $\langle P_i\rangle_\alpha = P_i^B$, we can define the upper bound F_i^B,

$$F_i^B = E_i + \frac{k_B T\langle P_i \ln P_i\rangle_\alpha}{\langle P_i\rangle_\alpha} \geqslant E_i + k_B T \ln P_i^B = F, \tag{A10}$$

which can be estimated from repeated HSMC probability determinations for the same configuration i.

In Eq. (19) we have defined an exact expression for Z that enables a direct estimation of the free energy denoted there as F^D [Eq. (20)]. We show that F^D is also well defined for HSMC as

$$F^D = k_B T \ln\left[\left\langle \sum_i P_i^B (P_i \exp[E_i/k_B T])\right\rangle_\alpha\right], \tag{A11}$$

where, using $\langle P_i\rangle_\alpha = P_i^B$ for any α,

$$\left\langle \sum_i P_i^B (P_i \exp[E_i/k_B T])\right\rangle_\alpha$$

$$= \sum_i P_i^B (\langle P_i\rangle_\alpha \exp[E_i/k_B T]) = \sum_i P_i^B\left(\frac{1}{Z}\right) = \frac{1}{Z}. \tag{A12}$$

Additionally, this identity implies a straightforward determination of Z (and therefore F) for the case of repeated trials on the same configuration i, which is simply given by

$$Z = \frac{\exp[-\beta E_i]}{\langle P_i\rangle_\alpha}. \tag{A13}$$

[1] D. L. Beveridge and F. M. DiCapua, Annu. Rev. Biophys. Biophys. Chem. **18**, 431 (1989).
[2] P. A. Kollman, Chem. Rev. (Washington, D.C.) **93**, 2395 (1993).
[3] W. L. Jorgensen, Acc. Chem. Res. **22**, 184 (1989).
[4] H. Meirovitch, in *Reviews in Computational Chemistry*, edited by K. B. Lipkowitz and D. B. Boyd (Wiley, New York, 1998), Vol. 12, p. 1.
[5] N. Metropolis, A. W. Rosenbluth, M. N. Rosenbluth, A. H. Teller, and E. Teller, J. Chem. Phys. **21**, 1087 (1953).
[6] B. J. Alder and T. E. Wainwright, J. Chem. Phys. **31**, 459 (1959).
[7] J. A. McCammon, B. R. Gelin, and M. Karplus, Nature (London) **267**, 585 (1977).
[8] A. Szarecka, R. P. White, and H. Meirovitch, J. Chem. Phys. **119**, 12084 (2003).
[9] R. P. White and H. Meirovitch, J. Chem. Phys. **119**, 12096 (2003).
[10] H. Meirovitch, Chem. Phys. Lett. **45**, 389 (1977).
[11] H. Meirovitch, Phys. Rev. B **30**, 2866 (1984).
[12] H. Meirovitch, M. Vásquez, and H. A. Scheraga, Biopolymers **26**, 651 (1987).
[13] H. Meirovitch, S. C. Koerber, J. Rivier, and A. T. Hagler, Biopolymers **34**, 815 (1994).
[14] A. J. Chorin, Phys. Fluids **8**, 2656 (1996).
[15] H. Meirovitch, J. Phys. A **16**, 839 (1983).
[16] H. Meirovitch, Phys. Rev. A **32**, 3709 (1985).
[17] H. Meirovitch, J. Chem. Phys. **111**, 7215 (1999).
[18] R. P. White and H. Meirovitch, Proc. Natl. Acad. Sci. U.S.A. **101**, 9235 (2004).
[19] W. L. Jorgensen, J. Chandrasekhar, J. D. Madura, R. W. Impey, and M. L. Klein, J. Chem. Phys. **79**, 926 (1983).
[20] S. Cheluvaraja and H. Meirovitch, Proc. Natl. Acad. Sci. U.S.A. **101**, 9241 (2004).
[21] H. Meirovitch and Z. Alexandrowicz, J. Stat. Phys. **15**, 123 (1976).
[22] T. L. Hill, *Statistical Mechanics Principles and Selected Applications* (Dover, New York, 1987).
[23] Z. W. Salsburg, J. D. Jacobson, W. Fickett, and W. W. Wood, J. Chem. Phys. **30**, 65 (1959).
[24] Z. Li and H. A. Scheraga, J. Phys. Chem. **92**, 2633 (1988).
[25] R. L. Coldwell, Phys. Rev. A **7**, 270 (1973).
[26] E. M. Gosling and K. Singer, Pure Appl. Chem. **22**, 303 (1970).
[27] R. H. Henchman, J. Chem. Phys. **119**, 400 (2003).
[28] M. P. Allen and D. J. Tildesley, *Computer Simulation of Liquids* (Clarendon, Oxford, 1987).
[29] J. C. Owicki, in *Computer Modeling of Matter*, edited by P. Lykos, ACS Symposium Series Vol. 86 (American Chemical Society, Washington, 1978), p. 159.
[30] W. L. Jorgensen, J. Phys. Chem. **87**, 5304 (1983).
[31] J. C. Owicki and H. A. Scheraga, Chem. Phys. Lett. **47**, 600 (1977).
[32] G. M. Torrie and J. P. Valleau, Chem. Phys. Lett. **28**, 578 (1974).
[33] G. M. Torrie and J. P. Valleau, J. Comput. Phys. **23**, 187 (1977).
[34] D. Levesque and L. Verlet, Phys. Rev. **182**, 307 (1969).
[35] M. Mezei, Mol. Simul. **2**, 201 (1989).
[36] J. K. Johnson, J. A. Zollweg, and K. E. Gubbins, Mol. Phys. **78**, 591 (1993).
[37] M. Mezei, S. Swaminathan, and D. L. Beveridge, J. Am. Chem. Soc. **100**, 3255 (1978).
[38] M. Mezei, Mol. Phys. **47**, 1307 (1982).
[39] M. Mezei, Mol. Phys. **61**, 565 (1987).
[40] W. L. Jorgensen, J. F. Blake, and J. K. Buckner, Chem. Phys. **129**, 193 (1989).
[41] J. Hermans, A. Pathiaseril, and A. Anderson, J. Am. Chem. Soc. **110**, 5982 (1988).
[42] Z. Li and H. A. Scheraga, Chem. Phys. Lett. **154**, 516 (1989).
[43] J. Quintana and A. D. J. Haymet, Chem. Phys. Lett. **189**, 273 (1992).
[44] M. Zacharias, T. P. Straatsma, and J. A. McCammon, J. Chem. Phys. **100**, 9025 (1994).
[45] C. Pangali, M. Rao, and B. J. Berne, Chem. Phys. Lett. **55**, 413 (1978).
[46] E. Prazen, *Modern Probability Theory and its Application* (Wiley, New York, 1960), p. 434.